OXFORD

Human Molecular Genetics, 2016, Vol. 00, No. 0 1–11

doi: 10.1093/hmg/ddw342
General Article

GENERAL ARTICLE

Impaired protein stability and nuclear localization of *NOBOX* variants associated with premature ovarian insufficiency

Ilaria Ferrari[1], Justine Bouilly[2,3], Isabelle Beau[2,3], Fabiana Guizzardi[1], Alberto Ferlin[4], Marzia Pollazzon[5†], Mariacarolina Salerno[6], Nadine Binart[2,3], Luca Persani[1,7*] and Raffaella Rossetti[1]

[1]Laboratory of Endocrine and Metabolic Research, IRCCS Istituto Auxologico Italiano, Milan, Italy, [2]Inserm U1185, Le Kremlin-Bicêtre, France, [3]Université Paris-Sud, Faculté de Médecine Paris-Sud, Le Kremlin-Bicêtre, France, [4]University of Padova, Department of Medicine, Unit of Andrology and Reproductive Medicine, Padova, Italy, [5]IRCCS Istituto Auxologico Italiano, Milan, Italy, [6]Department of Translational Medical Sciences, University Federico II, Naples, Italy, and [7]Department of Clinical Sciences & Community Health, University of Milan, Milan, Italy

*To whom correspondence should be addressed at: Luca Persani, MD PhD, San Luca Hospital, Piazzale Brescia 20 – 20149 Milan, Italy, luca.persani@unimi.it
†Current address: Clinical Genetics Unit, Obstetric and Paediatric Department, Arcispedale Santa Maria Nuova-IRCCS, 42123 Reggio Emilia, Italy

Abstract

Premature ovarian insufficiency (POI) is a clinical syndrome defined by a loss of ovarian activity before the age of 40. Its pathogenesis is still largely unknown, but increasing evidences support a genetic basis in most cases. Among these, heterozygous mutations in *NOBOX*, a homeobox gene encoding a transcription factor expressed specifically by oocyte and granulosa cells within the ovary, have been reported in ~6% of women with sporadic POI. The pivotal role of NOBOX in early folliculogenesis is supported by findings in knock-out mice. Here, we report the genetic screening of 107 European women with idiopathic POI, recruited in various settings, and the molecular and functional characterization of the identified variants to evaluate their involvement in POI onset. Specifically, we report the identification of two novel and two recurrent heterozygous NOBOX variants in 7 out of 107 patients, with a prevalence of 6.5% (upper 95% confidence limit of 11.17%). Furthermore, immunolocalization, Western Blot and transcriptional assays conducted in either HEK293T or CHO cells revealed that all the studied variants (p.R44L, p.G91W, p.G111R, p.G152R, p.K273*, p.R449* and p.D452N) display variable degrees of functional impairment, including defects in transcriptional activity, autophagosomal degradation, nuclear localization or protein instability. Several variants conserve the ability to interact with FOXL2 in intracellular aggregates. Their inability to sustain gene expression, together with their likely aberrant effects on protein stability and degradation, make the identified *NOBOX* mutations a plausible cause of POI onset.

Received: July 14, 2016. **Revised:** September 29, 2016. **Accepted:** September 29, 2016

J_ID: HMG Customer A_ID: DDW342 Copyedited by: PR Manuscript Category: General Article Cadmus Art: OP-HMGJ

Introduction

Premature ovarian insufficiency (POI) is a clinical syndrome defined by a loss of ovarian activity occurring in about 1% of women before the age of 40 (1), which is characterized by amenorrhea, hypoestrogenism, and high gonadotropin levels. Furthermore, one out of ten women aged between 40 and 45 suffers from early menopause (EM) (2). There are no currently available diagnostic tools to promptly predict the onset of the disease, and oftentimes patients are diagnosed when their oocyte reserve has already been severely compromised and, with that, their chances of conceiving (3).

Although common causes of POI include cytogenetic abnormalities of the X chromosome, as well as a history of endocrine autoimmunity, such pathology remains classified as idiopathic in most cases. A genetic basis for ovarian insufficiency is supported by the fact that a substantial number of cases (4–31%) are family linked (4,5), and so far an increasing number of genes have been identified to be mutated in women with POI, each one of those explaining no more than 3–6% of cases (6). Interestingly, some of those genes encode for transcription factors known to play pivotal roles in follicular physiology (7,8). One of those is the Newborn Ovary Homeobox (*NOBOX*, OMIM *610934) transcription factor, a homeodomain-containing, oocyte- and granulosa cell-specific protein (9,10) able to directly regulate the expression of key oocyte-specific factors such as Gdf9, Oct4 and KIT-L (11–14). In mice, NOBOX expression can be detected in embryonic ovaries as early as embryonic day 15.5, and its knock-out has been shown to cause female sterility due to accelerated postnatal oocyte loss and blockade in the primordial to primary follicle transition (11,15). Follicles are then replaced by fibrous tissue in female knockout mice in a manner similar to ovarian dysgenesis in women (11). Further corroborating the importance of NOBOX activity for folliculogenesis, heterozygous *NOBOX* mutations have been consistently reported in women with sporadic POI of African and Caucasian origin at a prevalence of ~ 6% (POF5, OMIM #611548) (14,16–19). Vice versa, mutations in the homeobox domain of NOBOX seem not to be common explanations for POI in Asian women (20,21). The aim of this study was to expand the screening for *NOBOX* mutations to a new large cohort of 107 unrelated women with sporadic POI and to evaluate the functional impact of both our novel variants as well as several of those previously reported, with the ultimate goal of better understanding the role of *NOBOX* mutations in the onset of Premature Ovarian Insufficiency.

Results

Novel NOBOX variants have been identified in a cohort of 107 women with sporadic premature ovarian insufficiency

A total of 107 women of European origin affected with idiopathic POI and with a normal 46,XX karyotype were included in this study. Genetic analysis of the entire coding sequence and intron-exon junctions of *NOBOX* identified three missense and one nonsense variants (see Table 1) in 7 patients of our series. The variants c.331G > A (p.G111R) and c.1354G > A (p.D452N) were previously reported (14,8,19), whereas variants c.454G > A (p.G152R) and c.1345C > T (p.R449*) are novel. All the variants are located outside the homeodomain, and were found in the heterozygous state.

The frequencies of all the identified variants in the POI population did not differ significantly from those reported in the Exome Aggregation Consortium Browser (ExAC) ($p > 0.05$, Fisher's exact test).

Table 1 lists all the identified variants in relation to the clinical manifestation. Particularly, patients 2 and 3, carrying variant p.G152R, both presented with a mild phenotype of EM, which onsets respectively at 44 and 45 years old, with oligomenorrhea starting from age 39 in the latter case. On the contrary, the earliest onset of the disease was in patient 7 (with primary amenorrhea) and patient 4 who, despite having experienced spontaneous menarche, was diagnosed with POI at age 14. The remaining patients experienced secondary amenorrhea.

In silico analysis

The results of the *in silico* analysis to predict the functional impact of the two novel variants are summarized in Table 2. Briefly, we used five different bioinformatic tools to predict their possible impact on protein structure and function. The p.R449* variant was predicted to be pathogenic with a high degree of confidence by all softwares, while the p.G152R variant was predicted to be damaging only by three of five tools.

POI-associated NOBOX variants impair transcriptional activity

The functional consequences of the variants found in our cohort (p.G111R, p.G152R, p.R449* and p.D452N) were evaluated in HEK293T cells on the human *OCT4* (Fig. 1) and *GDF9* (data not shown) promoters, both of which contain NOBOX binding elements. We observed a dramatic significant decrease in the transactivation of both reporter genes upon co- transfection with all the mutant constructs compared to the WT. Such results were confirmed on both reporter genes in CHO cells (Supplementary Material, Fig. S1).

POI-associated NOBOX variants impair nuclear trafficking and solubility in HEK293T cells

As NOBOX transcriptional activity on its DNA targets relies on its translocation inside the nucleus, we then conducted

Table 1. Clinical evaluation of the seven POI patients

Case	Phenotype[a]	Age at onset	Sequence Variation[b]	Location	Aminoacid variation	dbSNP ID	ExAC MAF (EUR)	POI Patients MAF	Reported in POI
1	SA	26	**c.331G>A**	Exon 4	p.G111R	rs571490209	0.002	0.005	14
2	EM	44	**c.454G>A**	Exon 4	p.G152R	rs201806397	0.008	0.009	Novel
3	EM	45							
4	SA	14	**c.1345C>T**	Exon 8	p.R449[a]	rs760393493	3.334e -05	0.005	Novel
5	SA	NA[a]	**c.1354G>A**	Exon 8	p.D452N	rs112190116	0.014	0.014	18
6	SA	40							
7	PA	–							

[a]EM: Early Menopause; PA: Primary Amenorrhea; SA: Secondary Amenorrhea; NA: data Not Available.

[b]NCBI reference sequence: NM_001080413.3.

J_ID: HMG Customer A_ID: DDW342 Copyedited by: PR Manuscript Category: General Article Cadmus Art: OP-HMGJ

Table 2. *In silico* analysis of the *NOBOX* novel variants

Software	Variant	
	p.G152R	p.R449*
Polyphen[a]	Possibly Damaging (0.949)	//
UMD Predictor [b]	Polymorphism (32)	Pathogenic (100)
Mut Taster[c]	Polymorphism (0,999)	Disease causing (0,999)
SNPs&GO[d]	Disease (1)	//
SIFT/Provean[e]	Deleterious (-2,983)	Deleterious (-389,7)

[a]http://genetics.bwh.harvard.edu/pph2/. Scores range from 0 (benign variant) to 1 (damaging variant).

[b]http://umd-predictor.eu/. The pathogenicity scores are assigned as follows: a value of less than 50 is associated with the prediction of a not pathogenic mutation annotated as "polymorphism," a value of 50 to 64 is associated with the prediction of a "probable polymorphism," a value of 65 to 74 is associated with the prediction of a "probably pathogenic" mutation, while a value above 74 is associated with the prediction of "pathogenic" mutation (38).

[c]http://www.mutationtester.org/. A value close to 1 indicates a 'high' security of the prediction.

[d]http://snps-and-go.biocomp.unibo.it/ The Reliability index has a range from 0 (unreliable) to 10 (reliable).

[e]http://sift.jcvi.org/. Variants are predicted to be deleterious if the score is below -2.5; otherwise they are classified as neutral.

immunolocalization experiments in HEK293T cells transiently transfected with the NOBOX constructs WT and mutants (p.G111R, p.G152R, p.R449* and p.D452N). We included in the present study two previously reported variants: p.R44L, which has been proposed as benign, and the POI-associated p.G91W (14). As NOBOX belongs to a family of transcription factors interacting with DNA through a homeodomain, the additional p.K273* mutant (termed ΔHomeodomain), truncated at the level of the DNA-binding homeodomain, was generated to be used as a fully inactive control (10). In order to ensure the detection of either strong or mild localization defects, confocal images were acquired for all constructs and processed with an ImageJ macro to quantify the nuclear-to-cytosolic eYFP signal ratio. As NOBOX nuclear localization signal is contained in its homeodomain (9), the ΔHomeodomain mutant showed a complete impairment in nuclear translocation compared to the WT. A moderate defect in nuclear localization was assessed for all variants (except for the p.R44L), but reached statistical significance only in case of variants p.G91W, p.G152R and p.D452N (Fig. 2A and B). Moreover, the p.G91W, p.G111R, p.G152R and p.D452N mutants displayed a significant tendency to form both intranuclear and cytosolic aggregates, as shown by the quantification in Fig. 2C and D. To assess whether the NOBOX protein mutants sequestered inside the aggregates still retained the capacity to interact with known NOBOX partners, the aggregation-prone variants ΔHomeodomain, p.G91W, p.G111R, p.G152R and p.D452N were cotransfected with a construct encoding for the well-known NOBOX interactor FOXL2 (10) in HEK293T cells, and their colocalization was evaluated with the ImageJ plugin JACoP. Indeed, the aggregates formed by variants p.G91W, p.G111R, p.G152R and p.D452N colocalized with FOXL2 punctate staining in 13-27% of aggregates-containing cells, (see Table 3). Such colocalization appears to be specific, as the aggregates formed by the ΔHomeodomain variant, which lacks the binding domain for FOXL2 (10), never co-localized with FOXL2 (see Fig. 3A and B).

Immuno-localization experiment conducted in CHO cells failed to detect any impairment in mutant NOBOX solubility or translocation to the nucleus except for the ΔHomeodomain variant, which was significantly retained in the cytoplasm (Supplementary Material, Fig. S2A and B).

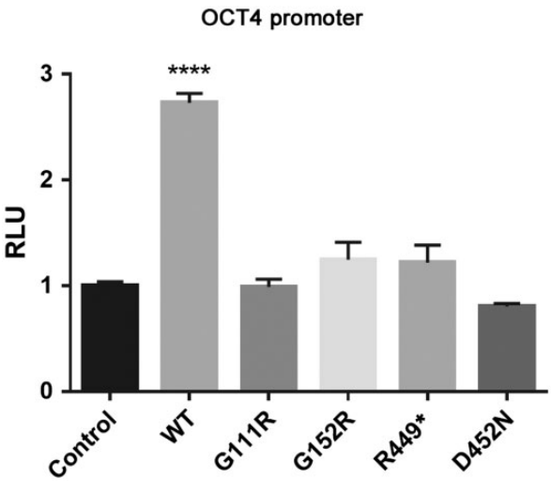

Figure 1. POI-associated *NOBOX* variants impair transcriptional activity. The transcriptional activity of WT NOBOX, p.G111R, p.G152R, p.R449* and p.D452N was studied with the use of *OCT4* promoter transfected in HEK293T cells. NOBOX activity is shown as the luciferase activity above baseline, which is defined as the activity observed in transfection with empty vector. Results are presented as mean ± s.e.m. of three independent experiments, each performed in sixplicates. $^{****}P < 0.0001$, RLU, relative light units.

In addition, we performed transcriptional assays using variants of NOBOX and wt FOXL2. All NOBOX variants do not exhibit any activity and in the presence of FOXL2 this activity is not rescued confirming that FOXL2 is trapped in the aggregates (see Fig. 3C).

POI-associated NOBOX variants alter protein stability

In order to clarify the molecular mechanisms responsible for the abnormal subcellular localization and the aggregates formation upon overexpression of NOBOX variants, the mutant proteins behavior was compared to the WT by Western blot experiments. In addition to a major band of the expected molecular weight for the WT and mutant proteins (bands FL, R449* and H in Fig. 3A), the anti-eYFP antibody recognized several smaller fragments, which were particularly evident in the case of the p.R449*, in which ~ 50% of the total eYFP-positive signal is restricted to a fragment of the apparent size of 46 kDa (band R449*-F1, see Fig. 3A and B). To assess whether such fragments could be a byproduct of protein turnover, we assessed WT and mutant NOBOX degradation pattern by treating cells with inhibitors of the two major proteolytic pathways, namely the ubiquitin-proteasome and autophagosome-lysosomal degradation.

Treatment with the proteasome inhibitor MG132 determined a strong increase in the signal of all eYFP-positive bands (Fig. 3C). The increase in the truncated fragments signal was accentuated in all the mutants compared to the WT protein, thus evidencing a partial proteolytic cleavage especially in case of variants p.R44L and p.G91W, which reached the statistical significance (see quantification in Fig. 3D).

Next, to investigate the potential role of lysosomal degradation in NOBOX clearance, we treated cells with NH_4Cl, which inhibits all types of lysosomal proteolysis. The amount of WT, p.G111R and p.G152R NOBOX mutants was increased by this

J_ID: HMG Customer A_ID: DDW342 Copyedited by: PR Manuscript Category: General Article Cadmus Art: OP-HMGJ

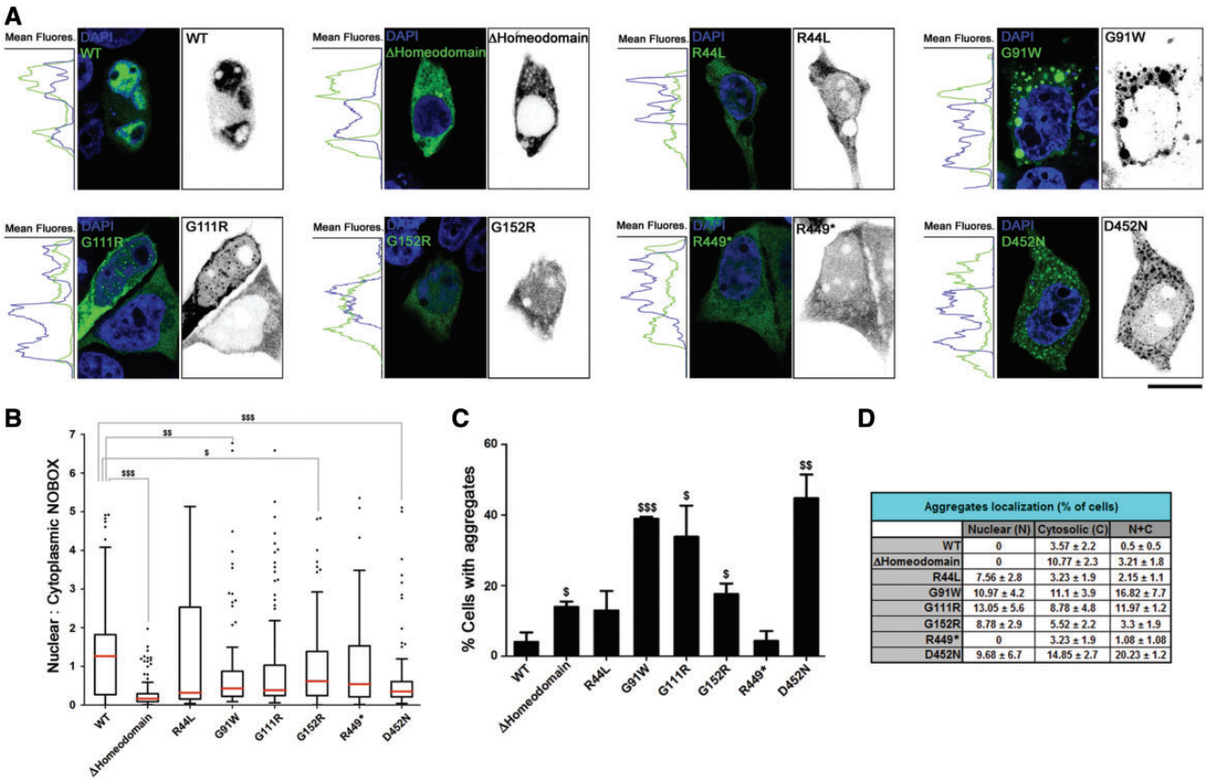

Figure 2. POI-associated *NOBOX* variants impair nuclear trafficking and solubility. (**A**) Laser confocal microscopy of HEK293T cells transfected with eYFP-tagged WT and mutant NOBOX (green). Nuclei were stained with DAPI (blue). For each transfectant, a representative merged image and the inverted green staining is shown. The plot profiles from regions of interests crossing the nuclei (as wide as the merged image and 10 pixels tall) were obtained with NIH ImageJ Software. Bar, 10 μm. (**B**) Box and Whiskers plot representing the nuclear-to-cytosolic NOBOX staining calculated from at least 90 cells from three different experiments for each transfectant. The Tukey method was applied to identify outlier values. The red lines represent the median values. (**C,D**) Quantification of the percentage of cells showing eYFP-positive aggregates ($n >$ 90 cells from three different experiments from each transfectant) in the nucleus (N), cytoplasm (C) or both (N+C). *P*-values: $: $P < 0.05$; $$: $P < 0.01$; $$$: $P < 0.001$.

Table 3. *In vitro* features of *NOBOX* mutants

Features	p.R44L	p.G91W	p.G111R	p.G152R	p.K273*[a]	p.R449*	D452N
Nuclear Localization Defects	No	Strong $P < 0.01$	Mild n.s.	Yes $P < 0.05$	Strong $P < 0.001$	Mild n.s.	Strong $P < 0.001$
Intracellular Aggregates	No	Strong $P < 0.001$	Yes $P < 0.05$	Yes $P < 0.05$	Yes $P < 0.05$	No	Strong $P < 0.01$
Colocalization between aggregates and FOXL2 signal	//	Yes (26,7%)[c]	Yes (16,7%)[c]	Yes (13,3%)[c]	No	//	Yes (26,7%)[c]
Inhibition of FOXL2 transcriptional activity	//	//	Yes $P < 0.01$	Yes $P < 0.01$	//	Yes $P < 0.01$	Yes $P < 0.01$
Appearance of Degradation Fragments (on WB)	Strong $P < 0.01$	Yes $P < 0.05$	Mild n.s.	Mild n.s.	Strong $P < 0.01$	Strong $P < 0.01$	Variable
Autophagosomal Degradation Impairment[b]	Yes	Yes	Variable	No	Variable	Yes	Yes
Defective Transcriptional Activity	No	Yes	Yes	Yes	Yes	Yes	Yes

n.s.: not significant.

[a]ΔHomeodomain.

[b]The scores were assigned as follow: Yes, resistance to both rapamycin autophagy induction and NH_4Cl mediated blockage; No, sensitivity to both rapamycin autophagy induction and NH_4Cl mediated blockage; Variable, discordant results between rapamycin and NH_4Cl treatments.

[c]The reported values (%) represent the percentage of NOBOX aggregates-bearing cells in which the colocalization between NOBOX aggregates and FOXL2 punctuate staining (calculated by Manders colocalization coefficiency) was > 5%. Data obtained from at least 30 cells from two different experiments for each transfectant.

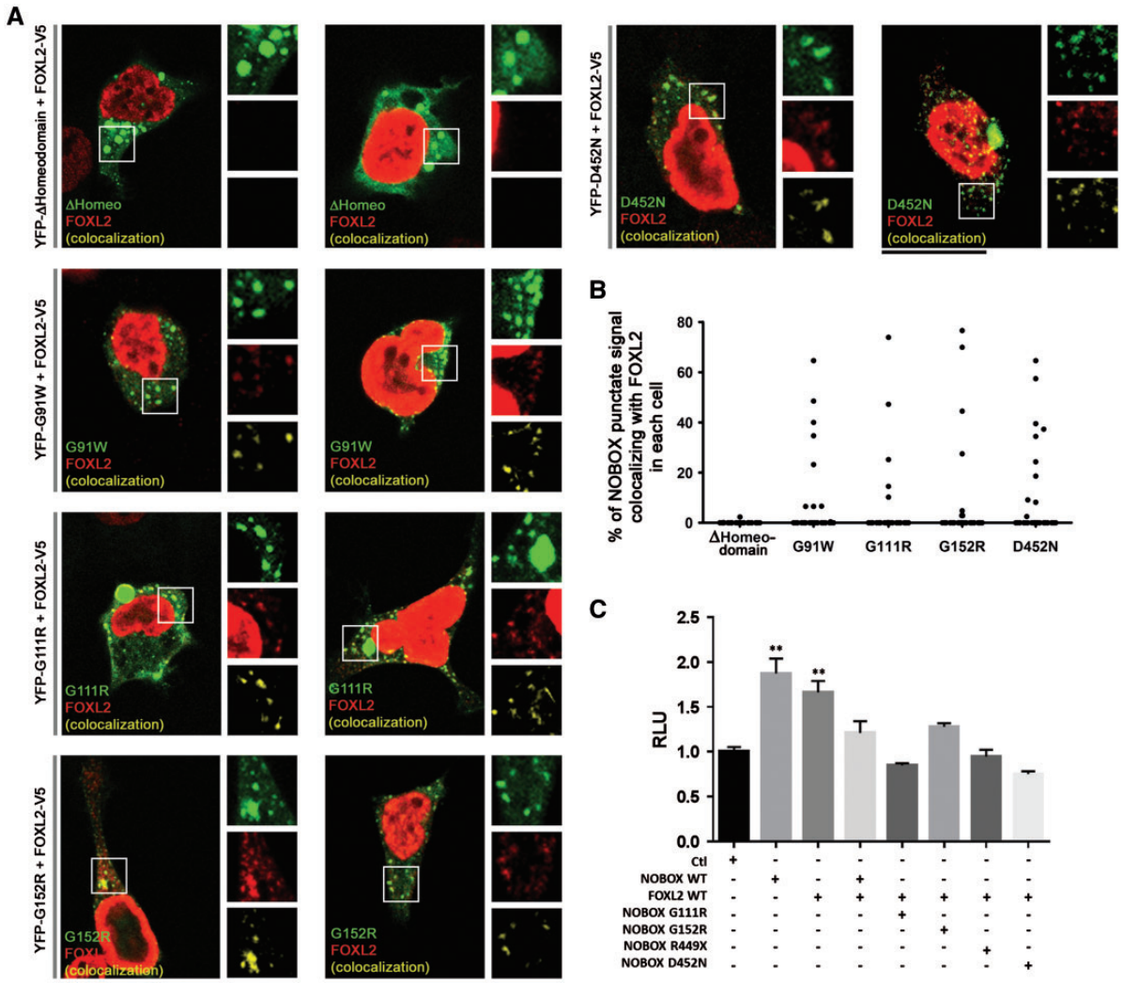

Figure 3. NOBOX aggregation-prone variants colocalize with FOXL2 in HEK293T cells. (**A**) Laser confocal microscopy of HEK293T cells co-transfected with eYFP-tagged NOBOX aggregation-prone variants (green) and V5-tagged FOXL2 (red). The constructs transfected in each images are indicated on the left. Nuclei were stained with DAPI (blue). For each transfectant, two representative merged images and 2X magnifications of the boxed areas are shown. The 2X magnifications represent the individual stainings for the eYFP (green) and V5 (red) signals, as well as the colocalization signal (yellow) obtained with NIH ImageJ function 'Image Calculator'. Bar: 10 μm. (**B**) Dot plot representing the percentage of colocalisation between the NOBOX signal localized in aggregates and the punctuate FOXL2 signal measured by Manders'colocalisation coefficient in 30 cells from two different experiments for each transfectant. Each single dot in the graph represents a cell. (**C**) The transcriptional activity of WT NOBOX, p.G111R, p.G152R, p.R449* and p.D452N was studied with the use of *OCT4* promoter transfected in HEK293T cells. NOBOX activity is shown as the luciferase activity above baseline, which is defined as the activity observed in transfection with empty vector. Results are presented as mean ± s.e.m. of three independent experiments, each performed in sixplicates. $^{**}P < 0.01$. ctl, control; RLU, relative light units.

treatment, suggesting that they are sensitive to lysosomal degradation. On the other hand, the p.R44L, p.G91W, p.R449* and p.D452N mutants were unaffected by NH_4Cl, unraveling a potential defect in their degradation (see blots and quantifications in Fig. 4A and B).

Since NH_4Cl treatment inhibits all types of lysosomal proteolysis (i.e. macroautophagy, microautophagy or chaperone-mediated autophagy), we further specifically investigated the involvement of macroautophagy by treating cells with the blocker 3-methyladenine (3-MA) (22). 3-MA treatment strongly impaired degradation of all NOBOX constructs, without any significant differences among WT and mutants (Fig. 4C and D). Treatment with autophagy-inducer rapamycin further determined a significant decrement in the amount of WT and p.G152R full-length bands, thus suggesting the involvement of autophagy in their degradation. Variants p.G91W, p.G111R and p.D452N, while partially resistant to rapamycin treatment, showed a significant decrease of the full-length bands upon starvation. On the contrary, variants p.R44L and p.R449* showed insensitivity to both autophagy inducers (Fig. 4E and F). The autophagosomal system appears to play a role only on full-length NOBOX clearance, as we saw no effects on the intensity of the intermediate fragments upon treatment with either NH_4Cl, 3-MA, rapamycin or starvation (Fig. 4A, C and E). While a more in depth analysis of NOBOX degradation patterns would broaden our knowledge on NOBOX turnover, such experiments are beyond the scope of this study.

Discussion

NOBOX is a transcription factor expressed in oocytes and granulosa cells with a fundamental role in primordial follicle

J_ID: HMG Customer A_ID: DDW342 Copyedited by: PR Manuscript Category: General Article Cadmus Art: OP-HMGJ

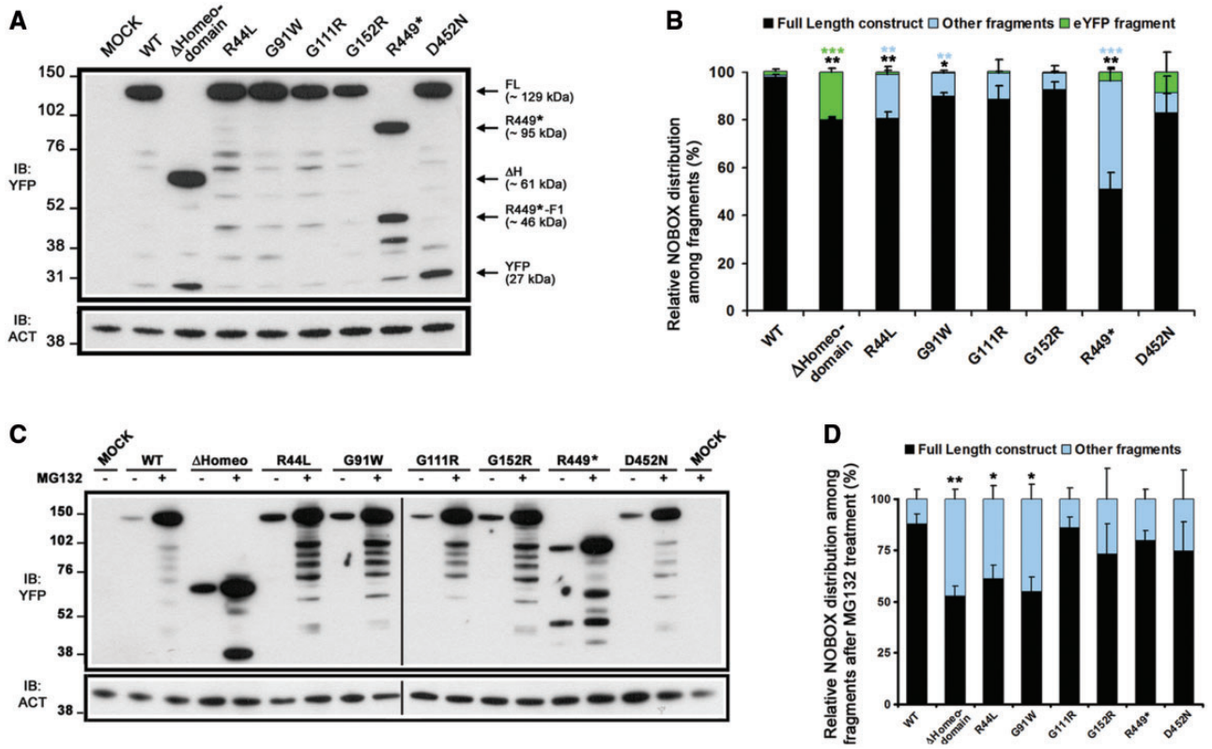

Figure 4. POI-associated *NOBOX* variants alter protein stability. (**A,B**) A representative Western blot of HEK293T cells transiently transfected with the indicated eYFP-tagged NOBOX constructs. The M16 empty vector was transfected as control (MOCK). The densitometric quantification of the relative abundance of NOBOX fragments in each transfectant is shown in panel B. Data are the mean ± s.e.m. of three indepenent experiments. The colored asterisks represent the statistical significance of WT vs mutants among the following groups: black for 'Full Length construct'; blue for 'Other fragments' and green for 'eYFP fragment'. (**C,D**) Representative immunoblot and densitometric quantification of the relative abundance of NOBOX fragments in each transfectant after treatment with 10 μM MG132 for 16 h prior to lysis. Twenty μg of protein lysates were loaded onto each lane. *P*-values: $^{*}P < 0.05$; $^{**}P < 0.01$; $^{***}P < 0.001$.

formation and primordial to primary follicle transition during ovarian folliculogenesis (11,15). In this study, we identified two known mutations (p.G111R and p.D452N) and two new variants, the missense mutation p.G152R and the nonsense mutation p.R449*, in a cohort of 107 European 46,XX women with POI, with a prevalence of 6.5% and an upper 95% confidence limit of 11.17%.

As the *in silico* analysis gave contrasting results, we carried out the molecular and functional characterization of these variants, as well as of four previously reported ones (p.R44L, p.G91W, p.G111R and p.D452N) (results summarized in Table 3).

The first experiments were aimed at the evaluation of the functional impact on transcriptional activity of the mutants in HEK293T cells, and revealed a total loss of transactivation on both *OCT4* and *GDF9* promoters for all variants found in our patients, including the already published, but never *in vitro* tested p.D452N mutation. The immunolocalization experiments on eYFP-tagged WT and mutant NOBOX in HEK293T cells further revealed an impaired nuclear localization for all variants, except for the p.R44L, which has already been proposed to represent a rare benign variant with a mild functional impact (14). This localization failure is associated with the appearance of intracellular aggregates in the case of variants p.G91W, p.G111R, p.G152R and p.D452N. As intracellular aggregates are usually degraded via autophagic pathways that converge on the lysosome, we treated cells with autophagy modulators such as NH_4Cl, 3-MA, rapamycin or serum starvation, which collectively demonstrated that WT NOBOX could be degraded via autophagy in HEK293T cells, which has never been reported in literature before. Concerning the aggregation-prone variants, the p.G91W and p.D452N displayed a significant degradation impairment compared to WT. This finding suggests that these aggregates are not degraded by autophagy process. Since NOBOX activity relies on its dimerization and all mutations were detected in the heterozygous state, the formation of these aggregates could be of particular interest for the POI pathology, as a higher tendency of the mutant proteins to aggregate may not only hamper their translocation to the nucleus, but may also lead to a partial sequestration of the wild-type counterpart. Such deleterious effect may be further worsened by the sequestration of additional NOBOX interactors into the aggregates, as indicated by the fact that the protein aggregates formed by NOBOX variants p.G91W, p.G111R, p.G152R and p.D452N colocalized with the known NOBOX interactor FOXL2 (10) upon cotransfection. The existence of a physical interaction in these cytoplasmic aggregates is supported by the conserved inhibition of FOXL2 wild-type transcriptional activity by the NOBOX variants (see Fig. 3). Interestingly, solubility defects have already been reported for variants of FOXL2 itself (24), whose mutations are also associated with POI (25).

Noteworthy, protein aggregation and cleavage defects have been reported to be implicated in ageing as well as in the onset of several degenerative pathologies (e.g. neurodegenerative diseases), where the formation of aggregates enhance the toxic effect of the mutant proteins (25). It is therefore not surprising that similar pathogenic mechanisms may be implicated in the

J_ID: HMG Customer A_ID: DDW342 Copyedited by: PR Manuscript Category: General Article Cadmus Art: OP-HMGJ

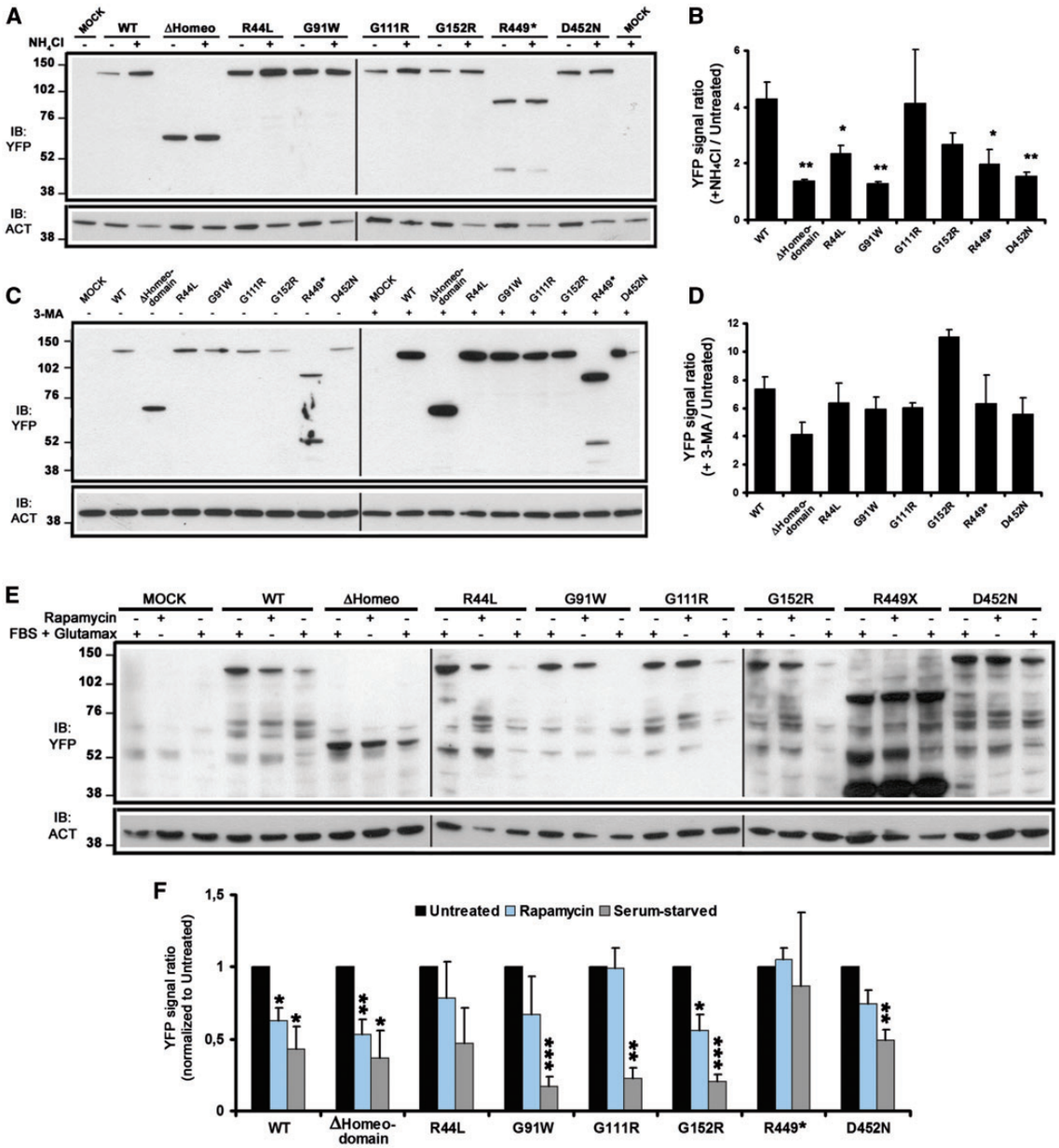

AQ8 **Figure 5.** POI-associated NOBOX variants alter protein clearance via autophagy. (**A–F**) Representative immunoblots and relative densitometric quantifications (expressed as ratios between treated and untreated) of HEK293T cells transfected with eYFP-tagged NOBOX constructs and treated with either 10 mM NH_4Cl (A,B), 10 mM 3-MA (C,D), 1 μM Rapamycin or serum starved (E,F) for 24 h prior to lysis. The P-values were calculated either versus WT (B,D) or versus the 'Untreated' of each transfectant (F). The M16 empty vector was transfected as control (MOCK). (A–F) Twenty μg of protein lysates were loaded onto each lane except for 3-MA-treated cells (C), for which 10 μg were loaded. Actin (ACT) was probed as a loading control. P-values: *$P < 0.05$; **$P < 0.01$; ***$P < 0.001$.

onset of POI, which may be considered as an accelerated ovarian ageing (26,27).

Degradation defects in the absence of aggregates were also seen for variant p.R449*. However, the impact of this nonsense mutation *in vivo* may be more complex, as it could either lead to the translation of a truncated protein devoid of biological activity or, given the position of the c.1345C > T transition in respect to the immature NOBOX mRNA, perhaps the trigger mutant mRNA degradation through nonsense-mediated RNA decay and ultimately lead to a haploinsufficency (28). Similarly, since all the *NOBOX* variants identified in our patients are in the heterozygous state, possible interactions could occur between wild-type and mutant proteins *in vivo*.

In contrast to the effects on mutant protein localization observed in HEK293T, we failed to detect any defect in mutants' trafficking in the epithelial cell line derived from the ovary of the Chinese hamster (CHO cells). However, it is widely known that nuclear permeability can be finely regulated by modulating the expression of the nuclear transport factors (29). In this regard, CHO cells might be more permissive to NOBOX nuclear

trafficking, thus preventing the detection of any defect in the mutants' translocation efficiency. In line with this hypothesis, unlike HEK293T, nuclear import of the wild-type protein itself seemed to be more efficient in CHO cells, whose nuclei never appeared completely devoid of NOBOX signal (see comparison between Fig. 2A and Supplementary Material, S2A). Such observation suggests the intriguing possibility that not only NOBOX expression but also its localization inside the cell may have a role in follicle differentiation, as already suggested for transcription factors involved in spermatogenesis (30). Indeed, the importance of the nuclear import system for follicle development has already been suggested by the fact that a missense mutation in the nuclear pore complex factor NUP-107 has been associated with 46,XX gonadal dysgenesis (31). Nevertheless, the striking impairment in mutant NOBOX transactivational capacity was confirmed in CHO cells. *In vitro* studies previously performed on two of the aggregation-prone variants p.G91W and p.G111R demonstrated the inhibition of transcriptional activity due to their absent DNA binding (14). Alternatively, the lack of reporter activation capacity in the absence of evidences of protein mislocalization and aggregation could be triggered either by the alteration of protein stability or by the loss of potential interaction with other factors through steric or electrostatic effects, a frequent phenomenon accounting for up to 80% of disease-associated aminoacid substitutions (32,33).

In our study, the phenotype of patients carrying the same mutation was often discordant, making it difficult to draw a clear genotype-phenotype correlation. For example, variant p.D452N remains of uncertain significance, since it displayed multiple defects in *in vitro* tests (see Table 3) despite being found with the same allele frequency in the ExAC browser. Moreover, heterozygous *NOBOX* p.D452N carriers manifested various degrees of ovarian dysfunction, ranging from primary to secondary amenorrhea. This lack of a correlation between genotype and the severity of the clinical manifestation has already been described in POI in case of some BMP15 mutations (34) as well as for NOBOX itself (14), thus strongly corroborating a model of complex pathogenesis (35) with variable penetrance in which one or more concurring variations in other predisposing gene or genes may further worsen the phenotype leading to an earlier disease onset, as recently shown by Bouilly and colleagues (19).

In contrast, the variant p.G152R displays a milder and more consistent phenotype, with both carriers affected by EM. The milder phenotype of the carriers is also in line with the formation of aggregates in the absence of degradation defects we saw in *in vitro* tests.

Overall, we show that the *NOBOX* variants p.G111R, p.G152R, p.R449* and p.D452N identified in our POI patients have an aberrant activity in *in vitro* tests. Their inability to sustain gene expression, together with the likely deleterious effects of protein aggregation, which may cause protein sequestration and defective degradation, makes them a plausible cause of POI onset in women with POI. Our data add to the mounting evidence supporting the importance of NOBOX activity in ovarian follicle physiology and further strengthens the need for geneticists working on POI to consider NOBOX screening a priority.

Materials and Methods

Patients and controls

A total of 107 women affected by idiopathic POI were included in this study. All the patients received a diagnosis of Premature Ovarian Insufficiency on the basis of the presence of amenorrhea for a period more than 6 months before the age of 40 years, together with two distinct measurements of plasmatic FSH levels in the postmenopausal range. All selected patients had a normal karyotype. Genetic investigation was extended to a cohort of 141 controls from the general population of the same ethnicity (84 females and 57 males). Institutional ethical committees approved the study, and informed consent for blood sampling and genetic investigations were obtained from all participants.

DNA sequencing

Genomic DNA was isolated from leukocytes of peripheral blood by using an automatic DNA extractor Tecan Freedom Evo (Tecan Group Ltd, Männedorf, Switzerland). Next generation sequencing of NOBOX entire coding sequence (i.e. exons 1-10) and intron-exon junctions was performed on 95 out of 107 by using miSeq instrument (Illumina, San Diego, CA, USA). Direct sequencing was also performed in the remaining cases. Reference sequences were obtained from NCBI (reference sequence: NM_001080413.3).

Constructs

The plasmid encoding V5-tagged FOXL2 has been described elsewhere (36). The eYFP-tagged plasmid encoding full-length human *NOBOX* (*Ensembl* database accession #ENST00000467773) was purchased from Genecopoeia (Rockville, MD, USA). The missense mutants p.R44L, p.G91W, p.G111R, p.G152R, p.D452N were obtained by site directed mutagenesis using the Agilent Quickchange II site-mutagenesis kit (Agilent Technologies, Santa Clara, CA, USA) starting from the wild-type (WT) construct. The non-sense variants ΔHomeodomain and p.R449*, as well as the M16-MOCK plasmid were obtained by subcloning from the original plasmid. All of the plasmid sequences were verified by means of direct sequencing to exclude unwanted substitutions.

Cell culture and transfection

HEK293T or CHO cells were cultured in DMEM (Dulbecco's Modified Eagle Medium) + Glutamax (Thermo Fisher Scientific, Waltham, MA, USA) supplemented with 1% penicillin-streptomycin and 10% foetal bovine serum (all from Sigma Aldrich, Saint Louis, MO, USA) at 37 °C and 5% CO_2, and transiently transfected using Fugene HD (Promega, Madison, WI, USA) according to the manufacturer's protocol.

Treatments

Autophagy and proteasome inhibitors were used at the following final concentrations: 10 μM MG132 (M7449, Sigma Aldrich), 10 mM NH_4Cl (A5666, Sigma Aldrich) and 10 mM 3-MA (M9281, Sigma Aldrich). Twenty-four hours after transfection, HEK293T cells were cultured for additional 24 h in Optimem + Glutamax (Thermo Fisher Scientific) with 1% FBS and supplemented with the indicated inhibitors. Twenty-four hours after transfection, HEK293T cells were cultured for additional 24 h with the autophagy inducer rapamycin (R8781, Sigma Aldrich) at 1μM concentration in DMEM + Glutamax. Serum starvation was performed 24 h after transfection by incubating HEK293T cells in DMEM (Thermo Fisher Scientific) for additional 24 h.

Immunoblotting

Cell extracts were solubilized in sodium dodecyl sulphate denaturation buffer. Equal amounts of extracted proteins were

separated on NuPage 4–12% BIS-TRIS gels (Thermo Fisher Scientific) and transferred onto nitrocellulose membranes (Thermo Fisher Scientific). Commercial primary antibodies were anti-actin (BD Biosciences, San Jose, CA, USA) and an anti-GFP against a common GFP/YFP epitope (Sigma Aldrich; listed as anti-YFP in the Results section), which we used to detect YFP-tagged constructs. Peroxidase-conjugated anti-mouse IgG (Thermo Fisher Scientific) was used as secondary reagent, and signals were visualized by means of an ECL Western blotting detection system (Millipore, Billerica, MA, USA). The densitometric quantification of signal intensities was performed by using the NIH ImageJ Software (NIH, Bethesda, MA, USA).

Reporter assays

The cells were cotransfected in 96-well plates by using FuGENE 6 (Promega), according to the manufacturer's protocol with 40 ng of NOBOX vector, 60 ng of promoter report vector, and 50 ng of the control vector containing Renilla luciferase, pRL-TK (Promega). Cells were lysed 48 h later with 1X passive lysis buffer (Promega). Firefly and Renilla luciferase activities were measured consecutively by using dual-luciferase assays (Promega) and a TriStar reader (Berthold, Bad Wildbad, Germany) and are expressed as relative light units (RLU). Each value is the average of six biological replicates, and each experiment shown is representative of at least five independent experiments.

HEK293T cells or CHO cells were transfected 48h with firefly luciferase promoter reporters (OCT4 or GDF9 or DK3 promoters), renilla vector, NOBOX and/or FOXL2 expression vectors or pcDNA3.1 vectors as control, as previously done (10,14).

Immunofluorescence microscopy

Forty-eight hours after transfection, HEK293T or CHO cells were fixed with 4% paraformaldehyde and mounted using ProLong Gold Antifade reagent (Thermo Fischer Scientific) containing DAPI for nuclei staining. For co-transfection experiments, HEK293T cells were fixed as described, stained with anti-V5 antibody (Novus Biologicals, Littleton, CO, USA) followed by goat anti-mouse Alexa Fluor 555 secondary antibody (Invitrogen Molecular Probes), and mounted with ProLong Gold Antifade reagent. Images were acquired using a Nikon EclipseTi-E inverted microscope with IMA10X Argon-ion laser System by Melles Griot (Nikon, Tokyo, Japan); all images were acquired with CFI Plan Apo VC 60X Oil (Nikon).

Image Analysis

Plot profiles in Fig. 2A were obtained using NIH ImageJ Software plot profile. The black and white images in Fig. 2A were obtained by inverting the signal of the green channel using Adobe Photoshop (Adobe Systems, San Jose, CA, USA).

To quantify the nuclear-to-cytosolic eYFP signal in NOBOX-transfected HEK293T or CHO cells, confocal images were processed with an ImageJ macro we generated as follows: briefly, the DAPI signal was processed with an automatic threshold to obtain a 'NUCLEUS' mask that we applied on the green channel to isolate the nuclear NOBOX signal. The green channel was also thresholded to isolate the whole NOBOX-positive cell. Nuclear and cell areas and total signal intensities were measured. For each cell, the signal ratio between the mean of nuclear and cytosolic eYFP signals was then calculated. At least 90 cells from three different experiments were analysed for each transfectant in case of HEK293T cells. For CHO cells, 60 cells from two different experiments were analysed for each transfectant.

The immunofluorescence images of HEK293T cells were also analysed for the appearance of intracellular aggregates by manually assessing at least 90 cells form three different experiments for each transfectant.

The magnifications showing the colocalization signal only in Fig. 3A was obtained with NIH ImageJ function 'Image Calculator', using the 'MIN' operation. To quantify NOBOX-FOXL2 colocalization, confocal images of HEK293T cells positive for both FOXL2 signal and NOBOX-positive aggregates were processed as follows: for each cell, the percentage of colocalisation between the NOBOX variant and FOXL2 inside the aggregates was obtained by calculating the Manders' colocalisation coefficient using ImageJ plugin JACoP (37). The thresholds for each image were modified manually to exclude the soluble cytosolic signal from the measurements. The signal from the nuclei was also excluded from the quantification. At least 30 cells from two different experiments were analysed for each transfectant.

Statistical Analysis

All quantitative data are presented as mean ± s.e.m (standard error of the mean). Each quartile value used to draw the box and whisker plot (Fig. 3B) represents itself the mean of at least three independent experiments. Multiple comparisons among groups were carried out by two-tailed Student's *t*-test, and in particular the Tukey Method was applied to identify outlier values in Fig. 2B, using GraphPad Prism software (GraphPad Software Inc., La Jolla, CA, USA). Statistical significance was indicated as follow: $^{*}P < 0.05$, $^{**}P < 0.01$, $^{***}P < 0.001$ and $^{****}P < 0.0001$.

Fisher's exact test was used in the analysis of a 2×2 contingency table reporting the allelic frequencies among groups (POI patients and ExAC European controls).

The upper 95% confidence limit for the proportion 7 out of 107 patients with POI has been calculated by using the *Stats Calculator* tool available at the web site https://www.mccallum-layton.co.uk/tools/statistic-calculators/confidence-interval-for-proportions-calculator/.

Supplementary Material

Supplementary Material is available at *HMG* online.

Acknowledgements

The authors would like to thank the POI patients and the control subjects who participated in this study and all the Clinical and Academic Hospitals providing samples.

Conflict of interest statement. None declared.

Funding

This work was supported by the Italian Health Ministry [GR-2011-02351636 to R.R.], and the IRCCS Istituto Auxologico Italiano [Ricerca Corrente Funds: 05C001_2010 to L.P.].

References

1. ESHRE Guideline Group on POI, Webber, L., Davies, M., Anderson, R., Bartlett, J., Braat, D., Cartwright, B., Cifkova, R., de Muinck Keizer-Schrama, S., Hogervorst, E., *et al.* (2016) ESHRE Guideline: management of women with premature ovarian insufficiency. *Hum. Reprod.*, **31**, 926–937.

2. Pelosi, E., Forabosco, A. and Schlessinger, D. (2015) Genetics of the ovarian reserve. *Front. Genet.*, **6**, 308.
3. Shelling, A.N. (2010) Premature ovarian failure. *Reproduction*, **140**, 633–641.
4. Persani, L., Rossetti, R. and Cacciatore, C. (2010) Genes involved in human premature ovarian failure. *J. Mol. Endocrinol.*, **45**, 257–279.
5. Chapman, C., Cree, L. and Shelling, A.N. (2015) The genetics of premature ovarian failure: current perspectives. *Int. J. Womens Health*, **7**, 799–810.
6. Qin, Y., Jiao, X., Simpson, J.L. and Chen, Z.J. (2015) Genetics of primary ovarian insufficiency: new developments and opportunities. *Hum. Reprod. Update*, **21**, 787–808.
7. Jagarlamudi, K. and Rajkovic, A. (2012) Oogenesis: transcriptional regulators and mouse models. *Mol. Cell Endocrinol.*, **356**, 31–39.
8. Lim, E.J. and Choi, Y. (2012) Transcription factors in the maintenance and survival of primordial follicles. *Clin. Exp. Reprod. Med.*, **39**, 127–131.
9. Suzumori, N., Yan, C., Matzuk, M.M. and Rajkovic, A. (2002) Nobox is a homeobox-encoding gene preferentially expressed in primordial and growing oocytes. *Mech. Dev.*, **111**, 137–141.
10. Bouilly, J., Veitia, R.A. and Binart, N. (2014) NOBOX is a key FOXL2 partner involved in ovarian folliculogenesis. *J. Mol. Cell Biol.*, **6**, 175–177.
11. Rajkovic, A., Pangas, S.A., Ballow, D., Suzumori, N. and Matzuk, M.M. (2004) NOBOX deficiency disrupts early folliculogenesis and oocyte-specific gene expression. *Science*, **305**, 1157–1159.
12. Choi, Y. and Rajkovic, A. (2006) Characterization of NOBOX DNA binding specificity and its regulation of Gdf9 and Pou5f1 promoters. *J. Biol. Chem.*, **281**, 35747–35756.
13. Bayne, R.A., Kinnell, H.L., Coutts, S.M., He, J., Childs, A.J. and Anderson, R.A. (2015) GDF9 is transiently expressed in oocytes before follicle formation in the human fetal ovary and is regulated by a novel NOBOX transcript. *PLoS One*, **10**, e0119819.
14. Bouilly, J., Roucher-Boulez, F., Gompel, A., Bry-Gauillard, H., Azibi, K., Beldjord, C., Dodé, C., Bouligand, J., Mantel, A.G., Hécart, A.C., *et al.* (2015) New NOBOX mutations identified in a large cohort of women with primary ovarian insufficiency decrease KIT-L expression. *J. Clin. Endocrinol. Metab.*, **100**, 994–1001.
15. Lechowska, A., Bilinski, S., Choi, Y., Shin, Y., Kloc, M. and Rajkovic, A. (2011) Premature ovarian failure in nobox-deficient mice is caused by defects in somatic cell invasion and germ cell cyst breakdown. *J. Assist. Reprod. Genet.*, **28**, 583–589.
16. Qin, Y., Choi, Y., Zhao, H., Simpson, J.L., Chen, Z.J. and Rajkovic, A. (2007) NOBOX homeobox mutation causes premature ovarian failure. *Am. J. Hum. Genet.*, **81**, 576–581.
17. Bouilly, J., Bachelot, A., Broutin, I., Touraine, P. and Binart, N. (2011) Novel NOBOX loss-of-function mutations account for 6.2% of cases in a large primary ovarian insufficiency cohort. *Hum. Mutat.*, **32**, 1108–1113.
18. Bouali, N., Francou, B., Bouligand, J., Lakhal, B., Malek, I., Kammoun, M., Warszawski, J., Mougou, S., Saad, A. and Guiochon-Mantel, A. (2016) NOBOX is a strong autosomal candidate gene in Tunisian patients with primary ovarian insufficiency. *Clin. Genet.*, **89**, 608–613.
19. Bouilly, J., Beau, I., Barraud, S., Bernard, V., Azibi, K., Fagart, J., Fèvre, A., Todeschini, A.L., Veitia, R.A., Beldjord, C., *et al.* (2016) Identification of multiple gene mutations accounts for a new genetic architecture of primary ovarian insufficiency. *J. Clin. Endocrinol. Metab.*:jc20162152.
20. Zhao, X.X., Suzumori, N., Yamaguchi, M.,. and Suzumori, K. (2005) Mutational analysis of the homeobox region of the human NOBOX gene in Japanese women who exhibit premature ovarian failure. *Fertil. Steril.*, **83**, 1843–1844.
21. Qin, Y., Shi, Y., Zhao, Y., Carson, S.A., Simpson, J.L. and Chen, Z.J. (2009) Mutation analysis of NOBOX homeodomain in Chinese women with premature ovarian failure. *Fertil. Steril.*, **91**, 1507–1509.
22. Vakifahmetoglu-Norberg, H., Xia, H.G. and Yuan, J. (2015) Pharmacologic agents targeting autophagy. *J. Clin. Invest.*, **125**, 5–13.
23. Caburet, S., Demarez, A., Moumné, L., Fellous, M., De Baere, E. and Veitia, R.A. (2004) A recurrent polyalanine expansion in the transcription factor FOXL2 induces extensive nuclear and cytoplasmic protein aggregation. *J. Med. Genet.*, **41**, 932–936.
24. Verdin, H. and De Baere, E. (2012) FOXL2 impairment in human disease. *Horm. Res. Paediatr.*, **77**, 2–11.
25. Labbadia, J. and Morimoto, R.I. (2015) The biology of proteostasis in aging and disease. *Annu. Rev. Biochem.*, **84**, 435–464.
26. Gagnon, A., Smith, K.R., Tremblay, M., Vézina, H., Paré, P.P. and Desjardins, B. (2009) Is there a trade-off between fertility and longevity? A comparative study of women from three large historical databases accounting for mortality selection. *Am. J. Hum. Biol.*, **21**, 533–540.
27. Cedars, M.I. (2013) Biomarkers of ovarian reserve-do they predict somatic aging?. *Semin. Reprod.*, **31**, 443–451.
28. Ottens, F. and Gehring, N.H. (2016) Physiological and pathophysiological role of nonsense-mediated mRNA decay. *Pflugers Arch.*, **468**, 1013–1028.
29. Yasuhara, N., Oka, M. and Yoneda, Y. (2009) The role of the nuclear transport system in cell differentiation. *Semin. Cell. Dev. Biol.*, **20**, 590–599.
30. Hogarth, C.A., Calanni, S., Jans, D.A. and Loveland, K.L. (2006) Importin α mRNAs have distinct expression profiles during spermatogenesis. *Dev. Dyn.*, **235**, 253–262.
31. Weinberg-Shukron, A., Renbaum, P., Kalifa, R., Zeligson, S., Ben-Neriah, Z., Dreifuss, A., Abu-Rayyan, A., Maatuk, N., Fardian, N., Rekler, D., *et al.* (2015) A mutation in the nucleoporin-107 gene causes XX gonadal dysgenesis. *J Clin Invest.*, **125**, 4295–4304.
32. Schuste, B. and Bateman, A. (2008) Protein interactions in human genetic diseases. *Genome Biol.*, **9**, R9.
33. Yue, P., Li, Z. and Moult, J.J. (2005) Loss of protein structure stability as a major causative factor in monogenic disease. *Mol. Biol.*, **353**, 459–473.
34. Rossetti, R., Di Pasquale, E., Marozzi, A., Bione, S., Toniolo, D., Grammatico, P., Nelson, L.M., Beck-Peccoz, P. and Persani, L. (2009) BMP15 mutations associated with primary ovarian insufficiency cause a defective production of bioactive protein. *Hum. Mutat.*, **30**, 804–810.
35. Toniolo, D. (2006) X-linked premature ovarian failure: a complex disease. *Curr. Opin. Genet. Dev.*, **16**, 293–300.
36. Georges, A., Benayoun, B.A., Marongiu, M., Dipietromaria, A., L'Hôte, D., Todeschini, A.L., Auer, J., Crisponi, L. and Veitia, R.A. (2011) SUMOylation of the Forkhead transcription factor

FOXL2 promotes its stabilization/activation through transient recruitment to PML bodies. *PLoS One*, **6**, e25463.

37. Bolte, S. and Cordelières, F.P. (2006) A guided tour into subcellular colocalization analysis in light microscopy. *J. Microsc.*, **224**, 213–232.

38. Frédéric, M.Y., Lalande, M., Boileau, C., Hamroun, D., Claustres, M., Béroud, C. and Collod-Béroud, G. (2009) UMD-predictor, a new prediction tool for nucleotide substitution pathogenicity – application to four genes: FBN1, FBN2, TGFBR1, and TGFBR2. *Hum. Mutat.*, **30**, 952–959.